Impaired peripheral nerve regeneration in type-2 diabetic mouse model

Vuong Minh Pham,[1] Nguyen H. Tu,[1] Tayo Katano,[1] Shinji Matsumura,[1] Akira Saito,[2] Akihiro Yamada,[3] Hidemasa Furue,[3] and Seiji Ito[1]

[1]Department of Medical Chemistry and [2]Clinical Research Laboratory, Kansai Medical University, 2-5-1 Shin-machi, Hirakata 573-1010, Japan

[3]Department of Neurophysiology, Hyogo College of Medicine, 1-1 Mukogawa-cho, Nishinomiya 663-8501, Japan

Correspondence: Dr. Seiji Ito, Department of Medical Chemistry, Kansai Medical University, 2-5-1 Shin-machi, Hirakata 573-1010, Japan.

Fax: +81-72-804-2349; e-mail: ito@hirakata.kmu.ac.jp

A running title: Delayed nerve regeneration in type-2 diabetic mice

Total number of pages	33
Figures	7
Tables	1

Total number of words

Whole manuscript	9,289
Abstract	247
Introduction	616

Comment
Reviewer 1

Key words: diabetic neuropathy; functional recovery; nerve regeneration; regenerative medicine

Conflict of interest

The authors declare no competing financial interests.

Acknowledgements

We greatly appreciate Drs. Shigeharu Wakana and Eiji Oka of Japan Mouse Clinic, RIKEN BRC for measurement of blood Hb1Ac. This work was supported in part by JSPS KAKENHI grant numbers 16H05233 and 26670291 to S.I., 16K09001 to T.K., and 15K08684 to S.M.

Author contribution

Performed experiments – VMP, NHT, AS, AY, HF. Experimental design and analysis – VMP, NHT, KT, SM, HF, SI. Manuscript preparation – VMP, SI.

Data Accessibility

All data can be fully available upon request to the corresponding author. (ito@hirakata.kmu.ac.jp).

Abbreviations

α-BTX, α-bungarotoxin; DAPI, 4’6-diamidino-2-phenylindole; DRGs, dorsal root ganglia; GCM, gastrocnemius muscle; GTT, glucose tolerance test; HE, hematoxylin and eosin; IENF, intraepidermal nerve fibers; NA, nicotinamide; NMJs, neuromuscular junctions; PBS, phosphate-buffered saline; PFA, paraformaldehyde; PGP9.5, protein gene product 9.5; PTEN, phosphatase and tension homolog; STZ, streptozotocin; YFP, yellow fluorescent protein

Abstract

Peripheral neuropathy is one of the most common and serious complications of type-2 diabetes. Diabetic neuropathy is characterized by a distal symmetrical sensorimotor polyneuropathy, and its incidence increases in patients 40 years of age or older. In spite of extensive research over decades, there are few effective treatments for diabetic neuropathy besides glucose control and improved lifestyle. The earliest changes in diabetic neuropathy occur in sensory nerve fibers, with initial degeneration and regeneration resulting in pain. To seek its effective treatment, here we prepared a type-2 diabetic mouse model by giving mice 2 injections of streptozotocin and nicotinamide and examining the ability for nerve regeneration by using a sciatic nerve transection-regeneration model previously established by us. Seventeen weeks after the last injection, the mice exhibited symptoms of type-2 diabetes, i.e., impaired glucose tolerance, decreased insulin level, mechanical hyperalgesia, and impaired sensory nerve fibers in the plantar skin. These mice showed delayed functional recovery and nerve regeneration by 2 weeks compared with young healthy mice and by 1 week compared with age-matched non-diabetic mice after axotomy. Furthermore, type-2 diabetic mice displayed increased expression of PTEN in their DRG neurons. Administration of a PTEN inhibitor at the cutting site of the nerve for 4 weeks promoted the axonal transport and functional recovery remarkably. The present study demonstrates that peripheral nerve regeneration was impaired in type-2 diabetic model and that its combination with sciatic nerve transection is suitable for the study of the pathogenesis and treatment of early diabetic neuropathy.

Introduction

Diabetes mellitus is a complex disorder of metabolism characterized by chronic hyperglycemia (Kerner & Brückel, 2014). There are 2 forms of this disease. Type-2 diabetes makes up more than 90% of the incidence of diabetes and is increasing not only in developed countries but also in developing ones as well (Bril, 2014; O'Brien *et al*., 2014). While type-1 diabetes results from a loss of insulin production by the destruction of the pancreatic β cells, the type-2 form is attributed to insulin resistance and relative insulin deficiency. In type-2 non-obese diabetes patients often found in East Asian countries such as Japan, China, and Korea, the reduction in insulin secretion is more important than the increase in insulin resistance. Peripheral neuropathy is the most common among complications; and typical diabetic neuropathy is a chronic, symmetrical, length-dependent sensorimotor polyneuropathy, known as a stocking-glove neuropathy, affecting 30-50% of diabetic patients (Tesfaye *et al*., 2010; Feldman *et al*., 2017). Although diabetic neuropathy is associated with increased morbidity and mortality, no effective treatments besides tight glucose control are in use in clinics. However, a Cochrane review for randomized controlled trials of enhanced glucose control in diabetic patients revealed that more aggressive glucose control had a significant preventive effect on neuropathy in type-1 diabetics but not in type-2 ones (Callaghan *et al*., 2012).

In biomedical research, *in vivo* animal models are critical for understanding the pathogenesis and elucidating treatment strategies for diabetic neuropathy. Since 1967, when a diabetic rodent model was first prepared by using alloxan to damage specifically pancreatic β cells and induce diabetes (Preston, 1967), many diabetic animal models have been developed in the fight against the incessantly increasing incidence of diabetes (Islam, 2013). Among them, streptozotocin (STZ)-induced diabetes is the most common approach to prepare diabetic mouse models because of being well-established, reproducible, and easy to optimize (O'Brien *et al*., 2014). To protect insulin-secreting cells against STZ, co-administration of nicotinamide (NA) is proposed to induce experimental diabetic rodent models (Islam & Wilson, 2012; Szkudelski, 2012). This STZ-NA model is widely used and recommended as a non-obese type-2 diabetic rodent model. Szkudelski (2012) also noted that, although diabetes may be easily induced by using STZ and NA, the doses of these compounds must be adjusted to obtain the appropriate severity of diabetes and optimized for the purpose of specific studies.

Comment Reviewer 1

The earliest changes in diabetic neuropathy occur in sensory nerve fibers, where nerve degeneration and regeneration exist concurrently in patients (Dyck & Gianini, 1996; Green *et al.*, 2010); and these changes produce pain such as hyperesthesia and allodynia followed by hypoalgesia and numbness. However, the involvement of peripheral nerve regeneration in the progress of diabetic neuropathy and its mechanism *in vivo* are still unknown. We recently established a sciatic nerve transection-regeneration model with a drug delivery system by using *thy1*-yellow fluorescent protein (YFP) transgenic mice expressing this fluorescent protein in their axons (Unezaki *et al*., 2009). This nerve regeneration mouse model allowed us to follow nerve regeneration with the same animals for several months and examine the effect of drugs on nerve regeneration *in vivo*. In the present study, we prepared type-2 diabetic mouse model according to the procedures reported previously (Nakamura *et al.*, 2006) and characterized the model, with the main focus on diabetic neuropathy. To seek treatment strategies for diabetic neuropathy, we applied the sciatic nerve transection-regeneration model to type-2 diabetic mice and examined the influence of type-2 diabetes on peripheral nerve regeneration. Since phosphatase and tensin homolog (PTEN) is known to block nerve regeneration in the nervous system (Park *et al*., 2008; Christie *et al*., 2010; Singh *et al*., 2014), we also examined the effect of a PTEN inhibitor on the functional recovery and nerve regeneration *in vivo*.

Materials and methods

Animals and preparation of diabetic animal model

Animal experiments were conducted in accordance with Japanese guidelines and regulations for scientific and ethical animal experimentation in 2006 and approved by the Ethics Committees of Kansai Medical University and Hyogo College of Medicine. A total of 124 mice were used in this study. C57BL/6J mice were purchased from SLC (Hamamatsu, Japan). *Thy1*-YFP transgenic mice were purchased from Jackson Laboratory [strain B6.Cg-Tg (*thy1*-YFP)16Jrs/J, stock number 003709], kept, and bred at Kansai Medical University for this study under conditions of a 12-h light/dark cycle, a constant temperature of 22 ± 2ºC, and 60 ± 10% humidity. They received food and water *ad libitum*. All efforts were made to reduce the number of animals in this study.

Type-2 diabetic mice were prepared by injections of a combination of STZ and NA according to the protocol reported previously by Nakamura *et al*. (2006). Briefly, 8-week-old mice were fasted overnight before administration of STZ and NA. NA was dissolved in physiological saline and *i.p*. injected at 240 mg/kg 15 min before STZ administration. STZ was dissolved in cold sodium citrate (0.1 M, pH 4.5) and *i.p.* injected at 100 mg/kg. The same doses of NA and STZ were *i.p.* injected again 2 days later. Control mice were *i.p* injected with the vehicle alone. Mice used 17 weeks after the STZ/NA and vehicle injection were designated as Type 2-Db 25W and Non-Db 25W, respectively. Ten-week-old mice without treatment were also used as young control mice (Non-Db 10 W).

Measurement of blood glucose and insulin, and glucose tolerance test (GTT)

Blood samples were collected from tail vein of non-fasted mice and blood glucose concentration were measured every week after STZ and NA injection. To confirm the preparation of type-2 diabetes, GTT was carried out before experiments and after axotomy. Mice were fasted overnight, and D-glucose was *i.p.* administered at a dose of 2.0 g/kg. The glucose concentration in the blood was measured by using a glucose assay kit (MS-FR201B, Terumo, Tokyo, Japan) at 30 min before and 30, 60, and 120 min after glucose administration.

For plasma insulin measurement, blood samples were collected from non-fasted mice and at 30 min before and 30 and 60 min after D-glucose administration when fasted mice were subjected to GTT. Blood samples were centrifuged at 1,200 x *g* for 20 min at 4 ºC and the supernatants (5 µl) were measured by using a mouse insulin ELISA kit (Shibayagi, Gunma, Japan).

Histochemistry

For histochemistry of the skin and pancreas, animals were anesthetized by *i.p.* pentobarbital (50 mg/kg) and transcardially perfused with 25 ml of cooled phosphate-buffered saline (PBS) and then with 4% paraformaldehyde (PFA). Pancreas and skin were collected and postfixed in 4% PFA at 4ºC overnight. The pancreas block, embedded in paraffin, and the skin one, embedded in optical cutting temperature (O.C.T.) compound, were cut into 10- and 20-µm-thick sections, respectively. The pancreatic sections were then de-paraffinized by immersion in decreasing graded concentrations of ethanol and subjected to hematoxylin and eosin (HE) staining or immunostaining. Images of pancreatic tissue stained with HE were captured by using a NanoZoomer HT digital slide scanner (Hamamatsu Photonics, Hamamatsu, Japan) at x 40 magnification.

For immunohistochemistry, the pancreatic sections were immersed in sodium citrate, pH 6.0, at 95ºC for 20 min to retrieve the antigen of interest. Then, the sections were incubated overnight at 4ºC with mouse anti-insulin (1:1000, Abcam, Cambridge, U.K.) and rabbit anti-protein gene product 9.5 (PGP9.5) (1:500, UltraClone Ltd., Cambridge, U.K.) antibodies as primary antibodies applied to pancreas and skin sections, respectively. The sections were then incubated for 2 h at room temperature with Alexa 594 goat anti-mouse (1:400, Molecular Probes, Oregon, USA) and Alexa 546 goat anti-rabbit antibodies (1:500, Molecular Probes) as the secondary antibodies applied to pancreas and skin sections, respectively. Then, immunostained sections were counterstained by using Vectashield mounting medium containing 4’6-diamidino-2-phenylindole (DAPI; Vector Laboratories, Burlingame, CA, USA). Immunofluorescence and YFP expression were visualized with a laser scanning confocal imaging system, LSM 700 (Carl Zeiss, Jena, Germany) with the appropriate secondary antibodies and counterstained by using Vectashield mounting medium containing 4’6-diamidino-2-phenylindole (DAPI; Vector Laboratories, Burlingame, CA, USA). Immunofluorescence and YFP expression were visualized with a laser scanning confocal imaging system, LSM 700 (Carl Zeiss, Jena, Germany).

For measurements of intraepidermal nerve fibers (IENF), 27 to 30 images were captured per mouse, and PGP9.5-positive fibers were quantified according to the study of Lauria *et al*. (2007). The nerves crossing the basement membrane of the epidermis were counted. The nerves that appeared as branches below or within the basement membrane were counted as 2, while the nerves that branched in the epidermis were counted as 1.

For histology of gastrocnemius muscle (GCM), after perfusion of PBS, the GCM was collected and postfixed in 4% PFA at 4ºC for 15 min. The GCMs were then incubated for 30 min at room temperature in PBS containing 0.1% α-bungarotoxin (α-BTX) conjugated with Alexa Fluor 555 (1:1000, Thermo Fisher Scientific, Waltham, MA, USA) and 1% Triton-X 100. Whole endplates and YFP-positive nerves fibers were visualized by the confocal microscope LSM 700, and z-stack images of each mouse were counted. The data were expressed as the % of innervated and reinnervated endplates to the total number of endplates before and after axotomy.

To compare the survival of sensory neurons in the dorsal root ganglia (DRG) in Non-Db 27W and Type 2-Db 27W mice treated with PTEN inhibitor or vehicle (n = 3/group), neurons were labelled with the fluorescent neuro-tracer, Fluoro-ruby (Molecular Probe, Eugene, OR, USA) as reported previously (Tu *et al*., 2016). In brief, the wound was reopened to expose the sciatic nerve at 11 weeks after axotomy and the proximal sciatic nerve end was transected by a sharp scissor. A parafilm was placed underneath the nerve to prevent the Fluoro-ruby from making contact with the surrounding tissues. A volume (5 μL) of 10% Fluoro-ruby mixed in gel foam (Pfizer Japan, Tokyo, Japan) was applied to the transection site for 30 min. The sciatic nerve in naive mice (n = 3) was cut and used as the control. At 3 days after Fluoro-ruby loading, L4, L5, and L6 DRGs were dissected after fixation as described above and the DRGs were counted in a whole-mount DRG obtained by preparing 13–22 image stacks (25-μm z-steps) obtained with a laser scanning confocal microscope (LSM 510; Carl Zeiss, Jena, Germany).

Transmission electron microscopy

Under anesthesia by *i.p.* pentobarbital (50 mg/kg), sciatic nerve samples were prepared from Non-Db 10W and 25W and Type 2-Db 25W mice (3 mice in each group) and analyzed by transmission electron microscopy according to the procedures by Onishi *et al*. (1974). Intact sciatic nerves were fixed *in situ* with 2% glutaraldehyde in 0.1 M cacodylate buffer (pH 7.4) containing 25 mM $CaCl_2$ for 15 min at room temperature and then isolated nerves were postfixed with the same fixing buffer for 105 min at room temperature. After having been rinsed in the cacodylate buffer (pH 7.4) containing 0.2M sucrose, the sciatic nerves were further post-fixed in 1% osmium tetroxide in the same buffer for 2 h at 4ºC. The post-fixed samples were then dehydrated by passage through increasing graded concentrations of ethanol, infiltrated with Poly/Bed 812 resin (TAAB Laboratories, Reading, UK), and then polymerized for 36 h at 4ºC. Ultra-thin sections (60-70 nm thickness) were cut and collected on copper grids to increase the level of contrast and contrast-

stained with uranyl acetate and lead citrate. The ultra-thin sections were analyzed by use of a JEM-1400A transmission electron microscope (JEOL, Tokyo, Japan). For quantitating the number of myelinated and unmyelinated nerves, 10 photos were investigated per mouse. For measuring areas of axon and myelin, 40-50 myelinated axons were randomly selected in 5 square regions of interest (55 μm x 55 μm), at the top left, top right, center, bottom left, and bottom right of 1 photo per mouse and 3 mice were analyzed. The g-ratio was calculated by dividing the diameter of the axon by the outer diameter of the myelinated fiber. All measurements were carried out by using ImageJ ver. 1.50.

Electrophysiology

The *in vivo* spinal extracellular recording from dorsal horn neurons were carried out with Type 2-Db 27W and age-matched Non-Db mice according to the procedures reported previously (Furue *et al.*, 1999; Furue 2012; Choi *et al*., 2017). Briefly, under anesthetia with urethane (1.2-1.5 g/kg, *i.p.*), thoracolumbar laminectomy was performed at the level of T12 to L2 to expose the lumbar enlargement of the spinal cord. The mouse was placed in a stereotaxic apparatus (Model ST-7M, Narishige, Tokyo, Japan). The surface of the spinal cord was irrigated with 95% O_2-5% CO_2 equilibrated with Krebs solution (in mM: 117 NaCl, 3.6 KCl, 2.5 $CaCl_2$, 1.2 $MgCl_2$, 1.2 NaH_2PO_4, 11 glucose, and 25 $NaHCO_3$) at 38 ± 1ºC. A tungsten electrode (impedance, 1 MΩ, A-M systems, Sequim, WA, USA) was advanced into the spinal dorsal horn using a micromanipulator (Model MHW-4, Narishige). Action potentials in the dorsal horn were extracellularly recorded with an AC differential amplifier (EX 1, Dagan, Minneapolis, MN, USA), and analyzed with Offline Sorter software (version 3, Plexon, Dallas, TX, USA). Cutaneous mechanical stimulation was applied to the hind limb, and the dorsal horn neurons in which action potential was elicited by the stimulation were used in this study. Electrical cutaneous stimulation (200 μs square pule, 0-5 mA) was then applied to the receptive field at 0.5-1 Hz by a bipolar electrode (0.25 mm tip diameter, 5 mm separation). When the electrical stimulus-evoked action potential had a constant latency (< 2 ms), the latency from the stimulus artifact was measured.

Sciatic nerve transection-regeneration mouse model

The sciatic nerve transection-regeneration mouse model was applied to Type 2-Db 25W, Non-Db 25W, and Non-Db 10W mice according to the procedure reported previously (Unezaki *et al*., 2009). In brief, after deeply anesthetized by *i.p.* pentobarbital (50 mg/kg), right sciatic nerve

was exposed and fully transected around the nerve proximal to the trifurcation at the mid-thigh. The proximal and distal stumps were inserted into a 7-mm-long silicone tube (inner diameter, 1 mm; wall thickness, 0.5 mm), with each stump sutured to the wall to leave the 5-mm-long gap between them. After closure of the wound, the mice were returned to their individual cages. The wound was daily treated by 10% povidone-iodine (Kenei Pharmaceutical Co., Ltd., Osaka, Japan) until completely healed.

PTEN inhibitor SF1670 (Sigma-Aldrich, St. Louis, MO, USA) was dissolved in physiological saline at a dose of 200 nM and continuously administered at a flow rate of 0.11 μl/h for 4 weeks with a catheter tube attached to an osmotic pump (Alzet, Cupertino, CA, USA) to the inside of the silicone tube of the sciatic nerve transection-regeneration model mice.

Behavioral test and in vivo imaging

Functional and morphological nerve regeneration was assessed according to the procedures reported previously (Tu *et al*., 2016). All mice were acclimated to the testing environment for 1 h before mechanical stimuli were applied. For functional nerve regeneration, the paw withdrawal thresholds were measured with calibrated von Frey filaments ranging from 0.02 to 4 g before and every week after axotomy. The effect of the PTEN inhibitor on behavior was examined in a blind manner.

For morphological nerve regeneration, *thy1*-YFP transgenic mice were used. They express YFP selectively in the nervous system and allow the visualization of proper plantar digital nerves. Under anesthesia with isoflurane (Wako Pure Chemical, Osaka, Japan), images of the right planta of experimental living mice were captured under fluorescent stereomicroscope (SZX16; Olympus, Tokyo, Japan) combined with a cooled CCD camera (Retiga Exi-C; QImaging, Surrey, BC, Canada) before and every week after sciatic nerve axotomy. The images were processed by QCAPTURE PRO software, and the number of branches of proper plantar digital nerves was counted by the naked eye.

Western blot

Dorsal root ganglia (DRGs) at L4 - L6 levels on both sides were collected from type-2 diabetic mice (n = 3) at 10 weeks after the second STZ and NA injection and from naive mice (n = 3) at the same age individually. The DRGs were homogenized with a Potter homogenizer in RIPA buffer containing protease inhibitor cocktail (Nacalai Tesque, Kyoto, Japan) and

phosphatase inhibitor (Nacalai Tesque). The homogenate (12 μg of total protein/lane) was subjected to SDS-PAGE (10% acrylamide) and then transferred to a PVDF membrane. After blockage for 1 h at room temperature with 5% (w/v) skim milk in TBS-T buffer consisting of 0.1% Triton X-100, 150 mM NaCl and 10 mM Tris-HCl (pH 7.5), the membrane was incubated overnight at 4°C with rabbit anti-PTEN antibody (1:1,000, Cell Signaling Technology, Danvers, MA, USA) and rabbit anti-vinculin antibody (1:10,000, Abcam, Cambridge, U.K.) as a loading control. After having been washed with TBS-T buffer, the membrane was incubated for 1 h with horseradish peroxidase-conjugated goat anti-rabbit IgG (1:15.000, Zymed) at room temperature. It was then washed 4 times with TBS-T buffer, after which the immunoreactivity was detected by use of an enhanced chemiluminescence detection kit (Chemi-Lumi One Super, Nacalai Tesque).

Statistical analyses

The results of insulin-positive cells (Fig. 1C), blood glucose and plasma insulin measurements (Fig. 1D - F), mechanical sensitivity (Figs. 2A and 6C), reinnervation of plantar nerve (Fig. 6B), number of intraepidermal nerve fibers (IENF) (Fig. 3B), length of IENF (Fig. 3C), electron microscopy (Fig. 4), and innervation and reinnervation to the endplates (Fig. 5B) were analyzed by one-way non-repeated ANOVA followed by Dunnett's *post hoc* test. The results of blood glucose (Fig. 1A), electrophysiology (Table 1), and expression of PTEN (Fig. 7B) were analyzed by two-tailed unpaired Student's t-test. The results of mechanical sensitivity (Fig. 7C) and number of neurons (Fig. 7E) were analyzed by two-way non-repeated ANOVA followed by Tukey's *post hoc* test. All statistical analyses were performed by GraphPad Prism 6.0. The data were expressed as the mean ± SD or SEM. $p < 0.05$ was considered as significant.

Results

Preparation and characterization of type-2 diabetic model by injection of STZ and NA

Type-2 diabetic model mice were prepared by two injections of a low dose of STZ and NA to 8-week-old mice at an interval of 2 days according to the procedures reported previously (Nakamura *et al.*, 2006). All mice injected by STZ and NA gained body weights from 25.9 ± 1.5 g at the injection to 29.5 ± 1.7 g at the 16th week and remained alive for a long time. The blood glucose level in a non-fasting state was significantly increased in STZ- and NA-injected mice as compared with vehicle injected mice from 6 weeks after the injection in control mice (Fig. 1A). At 16 weeks after the injection, the levels of non-fasting blood glucose were 231.4 ± 28.5 and 116.4 ± 10.7 mg/dl ($p < 0.0001$ by unpaired t-test) in STZ- and NA-injected and vehicle-injected mice, respectively. These mice at 17 weeks after injection of STZ and NA were designated as Type 2-Db 25W mice. Age-matched control mice with vehicle injection and 10-week-old mice without injection were designated as Non-Db 25W and Non-Db 10W mice, respectively, and these 3 groups were used in the following experiments.

To characterize Type 2-Db 25W mice, we stained the pancreas by HE and with anti-insulin antibody (Fig. 1B). Although the pancreatic islets of Langerhans showed a normal shape with HE staining in all groups, the immunoreactivity to anti-insulin antibody was apparently decreased in the Type 2-Db 25W mice (Fig. 1B). When insulin-positive cells in the pancreas were counted, Type 2-Db mice had a significantly lower percentage (mean ± SD, n = 3) of pancreatic β-cells (37.69 ± 6.53%) as compared with Non-Db 10W (69.00 ± 7.96) and Non-Db 25W (66.67 ± 6.43) control groups ($F_{2,7} = 18.96$, $p = 0.0030$; Fig. 1C).

Comment Editors

Consistent with the immunostaining with anti-insulin antibody, plasma insulin level in non-fasted Type 2-Db mice (554.7 ± 360.3 pg/ml) was significantly lower than that of age-matched-Non-Db 25W mice (1,021 ± 165.7) ($F_{2,12} = 4.446$, $p = 0.0256$; Fig. 1D).

Comment Editors

All mice were fasted 12 h overnight before measurement of blood glucose and plasma insulin. While blood glucose levels were not different at 30 min before glucose injection (Pre) among the 3 groups, the significant difference was found between Type 2-Db and Non-Db 25W groups at 30 min (528.3 ± 77.31 *vs.* 369.0 ± 48.44 mg/dl, $F_{2,8} = 5.266$, $p = 0.0257$), 60 min (494.0 ± 117.2 *vs.* 310.3 ± 98.80, $F_{2,8} = 6.079$, $p = 0.0445$), and 120 min (416.0 ± 135.7 *vs.* 128.0 ± 26.22, $F_{2,8} = 15.02$, $p = 0.0026$) after glucose injection (Fig. 1E). In accordance with increase in blood glucose, Type 2-Db group significantly decreased the plasma insulin level as compared with Non-

Comment Editors

Db 25W group at pre (67.0 ± 41.5 vs. 290.4 ± 79.0 pg/ml, $F_{2, 8} = 16.46$, $p = 0.0009$), 30 min (175.8 ± 139.3 vs. 575.8 ± 207.6, $F_{2, 8} = 6.644$, $p = 0.0134$) and 60 min (193.2 ± 129.1 vs. 532.1 ± 201.3, $F_{2, 8} = 4.482$, $p = 0.0309$) (Fig. 1F). However, there was no statistical difference in blood glucose and plasma insulin between Non-Db 10 and 25W groups at 30 and 60 min after glucose injection. There was no difference in blood glycated hemoglobin 1Ac among these 3 groups (data not shown). These results demonstrated that Type 2-Db 25W mice prepared by two injections of STZ and NA showed at least a type- 2 Db-like model of insulin depletion at 17 weeks after the injection.

Comment Editors

Characterization of diabetic neuropathy in Type 2-Db mice

To meet the criteria of diabetic neuropathy recommended by the Diabetic Neuropathy Study Group of EASD (Biessels *et al*., 2014), we first compared the withdrawal thresholds to mechanical stimuli of Type 2-Db 25W group with the other two groups. Whereas the Non-Db 10W and Non-Db 25W mice showed a withdrawal threshold of 0.45 ± 0.05 g and 0.56 ± 0.04 g, respectively, the Type 2-Db 25W ones responded to mechanical stimuli with a lower threshold of 0.16 g, indicative of mechanical hyperalgesia ($F_{2,15} = 45.55$, $p < 0.0001$; Fig. 2A).

To measure sensory nerve conduction in the sciatic nerve, we next employed *in vivo* spinal extracellular recordings of dorsal neurons (Furue, 2012; Choi *et al*., 2017). When stimulus intensity of the cutaneous repetitive electrical stimulation was gradually increased, action potentials having a constant latency (< 2 ms) were elicited in dorsal horn neurons of Non-Db 27W mice (Fig. 2B). The latency between the evoked action potential and the stimulus artifact was 7.51 ± 0.72 ms (n = 12, Table 1). In some instances, higher amplitude of the stimuli elicited action potentials with a longer latency ranging from 32.9-58.1 ms (Fig. 2B), suggesting that the action potentials in the dorsal horn with a longer latency is mediated by C-afferent fibers, because they have a slower conduction velocity and need higher stimulus electrical intensity to excite in comparison with A-afferent fibers (Yoshimura & Jessell, 1989; Uta *et al*., 2010). Action potentials were evoked in dorsal horn neurons of Type 2-Db 27W mice by cutaneous stimulus and the latency between the evoked action potential and the stimulus artifact was 7.90 ± 0.64 ms (n = 13). There was no significant difference in the latencies, mostly depending on peripheral nerve conduction, between Type 2-Db and Non-Db mice ($p > 0.05$). However, the cutaneous stimulus threshold of Type 2-Db 25W mice (0.51 ± 0.09 mA, n = 13) was significantly higher than that in Non-Db 25W mice (0.27 ± 0.04 mA, n = 12; $p = 0.0350$ by unpaired t-test) (Table 1), suggesting that the threshold for eliciting action potential in the periphery was increased in Type 2-Db 27W mice.

Consistent with this notion, few action potentials with longer latency as detected in Non-Db mice (Fig. 2B) were elicited in Type 2-Db 27W mice with our maximum stimulus intensity (5 mA).

Since the electrophysiological recordings suggested that sensory nerve endings in the skin might be impaired, the plantar skin below the 2nd, 3rd, and 4th toes of untreated *thy1*-YFP mice was collected from the 3 groups and skin innervation was evaluated by immunostaining for PGP9.5, a pan-neuronal marker (Fig. 3A). The number of IENF was 52.7 ± 2.2, 46.8 ± 2.7, and 35.6 ± 1.7/mm (the mean ± SD, n = 3) in Non-Db 10W, Non-Db 25W, and Type 2-Db 25W groups, respectively. As compared with that in the Non-Db 10W group, the number of IENF was significantly reduced in the Non-Db 25W group ($F_{2,6} = 43.56$, $p = 0.0029$) and it further decreased in the Type 2-Db 25W group ($F_{2,6} = 43.56$ $p = 0.0149$; Fig. 3B). However, no significant difference in the length of free nerve endings was found among the 3 groups (Fig. 3B). These results demonstrate that the number of IENF decreased with age and that Type 2-Db 25W mice showed a symptom of diabetic neuropathy.

Comment Editors

The morphometry of transverse sections of the sciatic nerve made at the mid-thigh level was furthermore analyzed by transmission electron microscopy. The morphology of the myelinated and unmyelinated axons of Type 2-Db 25W mice appeared the same as that of Non-Db 10W and 25W mice (Fig. 4A). In fact, there was no difference in the density of myelinated and unmyelinated axons (Fig. 4B) and area of axons and myelin and the g-ratio (Fig. 4C and D) among the 3 groups.

Neuromuscular junctions (NMJs) are formed by the innervation of skeletal muscle and have a function in transmission of signals from motor neurons to muscle fibers (Witzemann, 2006). Taking advantage of *thy1*-YFP transgenic mice, we used α-BTX, a neurotoxin with strong affinity for nicotinic acetylcholine receptors on endplates, to assess the influence of diabetes on the structure of NMJs of GCM. More than 95% of NMJs were normally formed in the GCM in all 3 groups (Fig. 5), thus suggesting that motor innervation was not affected in the Type 2-Db 25W mice.

Collectively, Type 2-Db 25W mice showed mechanical hyperalgesia by behavioral measure (Fig. 2A), impaired sensory nerve endings by physiological measure (Table 1) and decease in IEFN density by structural measure (Fig. 3B), demonstrating that Type 2-Db 25W mice meet the criteria of diabetic neuropathy. On the other hand, there was no obvious abnormalities in nerve trunks of the sciatic nerve (Fig. 4) and NMJs of motor neurons (Fig. 5) in Type 2-Db 25W mice.

Type-2 diabetic mice showed delayed functional recovery after sciatic nerve axotomy

To clarify the influence of type-2 diabetes on peripheral nerve regeneration, we applied the sciatic nerve transection-regeneration model to Type 2-Db 25W, Non-Db 10W, and Non-Db 25W mice. The nerve regeneration of proper plantar digital nerves was tracked *in vivo* by fluorescence stereomicroscopy based on the advantage of using *thy1*-YFP transgenic mice (Fig. 6A). Consistent with our recent report (Tu *et al.*, 2016), 6 plantar digital nerves began to be weakly observed in Non-Db 10W mice at 5 weeks; and all digital nerves, by 8 weeks, after axotomy. The nerve regeneration to the foot was delayed by 1 week in the Non-Db 25W mice and further delayed in the Type 2-Db 25W mice as compared with that in the Non-Db 10W mice (Fig. 6B). The number of regenerated nerves at the first detection was 1 or 2 at the 6th week after axotomy in the Type 2-Db 25W group. The delay in nerve regeneration was clear in this group at the 7th, 8th, and 9th week thereafter; but the delay was not statistically significant among the 3 groups. The most visible differences among them was at the 5th and 6th week after axotomy ($F_{2,12}$ = 22.05, p = 0.0002; Non-Db 25W *vs*. Non-Db 10W at 5th week; $F_{2,12}$ = 12.77, p = 0.0141; Non-Db 25W *vs*. Type 2-Db 25W at 6th week). Whereas all plantar digital nerves were detected in Non-Db 10W mice (n = 4) at the 7th week, the average number of regenerated nerves was 9.80 ± 0.18 and 9.17 ± 0.65 in Non-Db 25W (n = 5) and Type 2-Db 25W (n = 6) mice, respectively, even at the 11th week. The variation in nerve regeneration speed seemed to be larger among mice in the Type 2-Db 25W group.

Comment Editors

We next assessed the functional recovery by measuring the withdrawal response to calibrated von Frey filaments applied to the right plantar surface. The mechanical force of 4 g was used as the cut-off value. Before right sciatic nerve transection, all mice responded to mechanical stimulation with a threshold of less than 0.6 g; and the Type 2-Db 25W mice exhibited mechanical hyperalgesia (Fig. 6C). No response to the von Frey filaments was found in any of the groups during the first 4 weeks after axotomy. The Non-Db 10W group began to respond to mechanical stimuli at 5th week after axotomy, and the threshold returned to the initial one at the 6th week ($F_{2,12}$ = 30.66, p = 0.0002 at 5th week; $F_{2,12}$ = 7.93, p = 0.0366 at 6th week; Fig. 6C). Similar to the time course of nerve regeneration, the response to mechanical stimuli was delayed by 1 week in Non-Db 25W group and further delayed in the Type 2-Db 25W group. The time course of functional recovery varied among 6 mice in the Type 2-Db 25W group and all mice returned to the normal level at 10th week. Interestingly, after a full recovery, i.e., a return to the initial threshold, all groups continued dropping their withdrawal thresholds to 0.16 g (Fig. 6C), suggesting that the injured nerves may have been hyperalgesic during the course of the functional

Comment Editors

recovery. In accordance with the recent report by Tu *et al.* (2016), there was a positive correlation between nerve regeneration *in vivo* (Fig. 6B) and the improvement of functional recovery after axotomy (Fig. 6C).

Next we analyzed the reinnervation in the skin and GCM and the morphometry of regenerated sciatic nerves at 11 weeks after axotomy, once functional recovery had completed (Fig. 6C). Whereas regenerated plantar digital nerves were detected under a fluorescence stereomicroscope at the 11th week after axotomy, the immunological activity of PGP9.5 in the skin collected from the same mice was hardly detectable (Fig. 3A), revealing that slow regeneration of IEFN, i.e., the free nerve endings of sensory neurons, mainly unmyelinated C-fibers, occurred in the skin after axotomy. As was shown in Fig. 3B, the number of IENF per mm epidermis was dramatically decreased in all groups: to 3.33 ± 0.99, 1.95 ± 2.82, 8.33 ± 6.42 in Non-Db 10W, Non-Db 25W, and Type 2-Db 25W, respectively. Similarly, the length of regenerated free nerve endings was 0.052 ± 0.03, 0.047 ± 0.071, and 0.231 ± 0.194 μm/100 μm^2 in Non-Db-10W, Non-Db 25W, and Type 2-Db 25W, respectively, being remarkably short as compared with that before axotomy (Fig. 3C).

In contrast, almost all endplates were reinnervated and NMJs had formed at 11 weeks after axotomy in all 3 groups as observed before axotomy (Fig. 5). Consistent with clinical symptoms of patients with type-2 diabetes (Feldman *et al.*, 2017), these results suggest that sensory nerves are more vulnerable and resistant to regeneration than motor nerves.

Collectively, these behavioral and morphological results showed that the regeneration of sensory nerves was delayed with respect to age and diabetes and that the sensory nerves were more affected than the motor ones.

Involvement of PTEN in the delay of nerve regeneration in Type 2-Db mice

The involvement of PTEN in attenuation of nerve regeneration was noted in recent reports showing that PTEN deletion significantly promotes regeneration of peripheral axons (Christie *et al.*, 2010). Therefore, we first compared the expression of PTEN protein in L4 - L6 DRGs taken from 3 naive mice and 3 Type 2-Db mice by performing Western blotting. As shown in Fig. 7A and B, all 3 diabetic mice showed significantly increased expression of PTEN protein in their DRGs.

Next we examined the effect of a PTEN inhibitor on nerve regeneration by using the sciatic nerve transection-regeneration model and an osmotic pump containing 200 nM PTEN inhibitor.

Instead of 25-week-old mice, 16-week-old ones were used in this experiment. Whereas neither vehicle-treated Non-Db nor Type 2-Db mice (n = 6) responded to the von Frey filaments by 5 weeks after axotomy, as was shown in Fig. 6C, the administration of the PTEN inhibitor prompted a response to them regardless of diabetes induction. Surprisingly, some of the 6 mice treated with the PTEN inhibitor responded as early as 3 weeks after axotomy; and the response returned to the level before axotomy at 7 weeks (Fig. 7C). Thus, it is evident that the PTEN inhibitor promoted the functional recovery after sciatic nerve regeneration in both Type 2-Db groups ($F_{1,20}$ = 28.54, vehicle *vs*. PTEN inh. $p = 0.0033$ at 5th week; $F_{1,20}$ = 19.00, $p = 0.0010$ at 6th week; $F_{1,20}$ =29.71, $p < 0.0001$ at 7th week; $F_{1,20}$ = 16.71, $p = 0.0029$ at 8th week) and Non-Db groups ($F_{1,20}$ = 28.54, vehicle *vs*. PTEN inh. $p = 0.0109$ at 5th week).

To investigate the effect of PTEN inhibitor on nerve regeneration after axotomy, we labelled sensory neurons in the DRG by the proximal application of Fluoro-ruby, a hydrophilic neuro-tracer to the transected sciatic nerve. Fig. 7D shows representative images of labelled L5 DRG neurons of Type 2-Db and Non-Db mice before and 8 weeks after axotomy. The number of labelled sensory neurons was 1,742 ± 627.3 in the intact L3 - L5 DRGs of Type 2-Db mice ($F_{2,12}$ = 23.35, $p = 0.0100$). The number of labelled neurons were significantly reduced by axotomy (491.3 ± 80.0) and this reduction was alleviated by treatment with PTEN inhibitor (1,484 ± 200.6) (Fig. 7E). Similarly, the number of labelled neurons (2,117 ± 521.1) were markedly reduced in Non-Db mice by axotomy (591.0 ± 161.2) and this reduction was alleviated by treatment with PTEN inhibitor (1,306 ± 136.3). These results demonstrated that PTEN inhibitor may promote the axonal transport in the axon regardless of diabetes.

Comment Editors

Discussion

STZ is a common chemical used to induce diabetic animal models based on its specific effect on pancreatic β-cells, and many diabetic animal models have already been established by using it (Van Belle *et al*., 2009). Because type-2 diabetes makes up more than 90% of diabetes cases and a majority of diabetic patients are lean in the East Asia, in the present study, we prepared type-2 diabetic model mice essentially according to the procedure reported by Nakamura *et al*. (2006). All mice injected twice with STZ at 100 mg/kg and NA at 240 mg/kg remained alive for more than 6 months and maintained a constant body weight without insulin supplementation. They increased blood glucose level and decreased plasma insulin level in a non-fasting state (Fig. 1A and D). This model showed a significant decrease in the insulin-positive cell population (Fig. 1B and C) and successful preparation of this type-2 diabetic model was confirmed by performing the GTT (Fig. 1E). Of these mice, 85% of them exhibited diabetic signs in the GTT at 17 weeks after STZ and NA injections; and this incidence gradually increased later. Furthermore, they showed neuropathic complications caused by diabetes, including mechanical hyperalgesia (Fig. 1D) and a decrease in the number of IENF in the skin (Figs. 3A and B). We also measured sensory nerve conduction by *in vivo* patch of spinal dorsal horns and demonstrated that sensory nerve endings might be impaired (Fig. 2B and Table 1). Since at least 2 of 3 measures, i.e. behavior, structure and physiology, are statistically different between Type 2-Db 25W mice and age-matched Non-Db 25W mice, our type-2 diabetic model met the criteria of diabetic neuropathy recommended by the Diabetic Neuropathy Study Group of EASD (Biessels *et al*., 2014). Although Type 2-Db 25W mice showed an impaired GTT (Fig. 1E and F), it showed normal hemoglobin 1Ac level, sensory nerve conduction (Table 1) and nerve trunk structure by electron microscopy (Fig. 5). Because these glycosylated hemoglobin 1Ac and nerve pathological changes are a nature of chemical reaction, rather than biological response induced by diabetes, they need a long period as with diabetic patients or high glucose concentration as with type-1 diabetic mice. Therefore, the present study first demonstrates that the Type 2-Db model has a merit of pursuing early changes of diabetic neuropathy because of high survival rates without insulin supplementation and reproducible preparation of type-2 diabetic model in mice. Furthermore, the preparation of Type 2-Db mice by STZ and NA injections without a high-fat diet is relatively inexpensive and suitable for studies on the pathogenesis and treatment of type-2 patients in East Asian countries.

Consistent with the results by Magill *et al.* (2007) showing that the tibial nerve returns to a 1:1 terminal axon to motor endplate ratio by 6 weeks after a sciatic nerve crush, the present results showed that there was no significant change in the structure of NMJs among Type 2-Db and Non-Db groups irrespective of sciatic nerve axotomy (Fig. 5). Our results demonstrated that the Type 2-Db model employed here did not exhibit motor disorders and that NMJs between motor endplates and terminal axons had properly formed in both Type 2-Db and Non-Db groups. Since motor dysfunction with distal weakness of the toes is known to occur much later in the course of diabetic neuropathy in humans, these findings support our contention that this Type 2-Db model without motor disorder is appropriate for diabetic neuropathy. Feldman *et al.* (2017) explains the difference in vulnerability to diabetes between sensory and motor neurons as follows: Whereas DRG neurons lie outside of the blood-brain barrier, motor neurons are localized in the ventral horn of the spinal cord under the protection of this barrier.

In the sciatic nerve, there are thin unmyelinated axons known as C-fibers or small fibers and myelinated A-fibers. Many anatomical studies demonstrate that the earliest changes in diabetic neuropathy occur at the level of the unmyelinated C-fibers, with initial degeneration and regeneration of C-fibers resulting in hyperalgesia (Green *et al.*, 2010). In fact, the most common early symptom of diabetic neuropathy is bilateral and symmetric damage with a distal-to-proximal gradient of severity, known as a stocking-glove neuropathy. This seemed to be the case with our Type 2-Db 25W model mice. When sensory nerve endings were immunostained with anti-PGP9.5 antibody, the number of IENF was significantly decreased in the Type 2-Db 25W group in Type 2-Db 25W mice (Fig. 3). This decrease in the number of IENF was supported by the electrophysiological findings that few action potentials with longer latency mediated by C-afferent fibers were elicited in Type 2-Db mice even with our maximum stimulus intensity at 5 mA. Although regenerated plantar digital nerves were detected under a fluorescence stereomicroscope at the 11th week after axotomy (Fig. 6A), the regeneration of IENF in the skin collected from the same mice was marginal (Fig. 3B). Because unmyelinated C-fibers lack the protection and nutrient supplementation afforded to myelinated sensory and motor axons by Schwann cells, these unmyelinated C-fibers are likely to be more susceptible to pre-diabetic conditions. On the other hand, the latency between stimulus in the skin and evoked action potential in spinal dorsal horn neurons was the same between Type2-Db and Non-Db mice (Table 1). There was no difference in the number of nerve, areas of axon and myelin, and the g-ratio of sciatic nerve trunks among the 3 groups by electron microscopy (Fig. 4). Although Type 2-Db mice did not exhibit the dramatic

fiber loss and demyelination documented in human diabetic neuropathy, whether the first target is thin C-fibers or pan nerve fibers needs further study.

PTEN is known to be a key member playing a role in the PI3K/Akt pathway through inhibition of PI3K, resulting in attenuated regrowth of axons (Park *et al.*, 2008). In fact, there have been many studies proving that activation of PTEN plays an attenuating role in nerve regeneration in both central and peripheral nervous system. Singh *et al.* (2014) found a significant increase in the expression of PTEN in sensory neurons and showed that the knockdown of PTEN in diabetic neurons accelerates the electrophysiological recovery and myelinated axon regrowth and skin reinnervation. In the present study, after confirming an increase in PTEN expression in the Type 2-Db mice (Fig. 7A and B), we examined the involvement of PTEN in nerve regeneration in the nerve transection-regeneration model (Fig. 7C). Unexpectedly, compared with the groups treated with the vehicle, the PTEN inhibitor accelerated the functional recovery in both Non-Db and Type 2-Db groups at 200 nM. Some mice in both Non-Db and Type 2-Db groups treated with the PTEN inhibitor responded to von Frey filaments at 3 weeks after axotomy. Consistent with this, decreased Fluoro-ruby labelling of DRG neurons after axotomy was markedly attenuated by the PTEN inhibitor in both Type 2-Db and Non-Db mice (Fig. 7D & E), suggesting that PTEN inhibition may accelerate nerve regeneration regardless of diabetes induction. Since insulin is known to promote nerve regeneration, the decrease in insulin level in Type 2-Db mice (Fig. 1D and F) may partially explain the delay in nerve regeneration in the mice.

In conclusion, for the treatment of diabetic neuropathy, the most effective method is a combination of prevention of the progression of diabetic symptoms and nerve degeneration with promotion of nerve regeneration (Yasuda *et al*., 2003). In the present study, we prepared our Type 2-Db mouse model by giving mice 2 injections of STZ and NA at a 2-day interval, which met the criteria recommended for assessment of diabetic neuropathy models by Diabetic Neuropathy Study Group of EASD (Biessels *et al*., 2014) and the Diabetic Complications Consortium for assessing diabetic neuropathy in mice (O'Brien *et al.*, 2014). Therefore, a combination of this model and sciatic nerve transection-regeneration model is suitable for the study of the treatment of pre-diabetic and early stages of diabetic neuropathy in humans, known as stocking-glove neuropathy.

References

Biessels, G.J., Bril, V., Calcutt, N.A., Cameron, N.E., Cotter, M.A., Dobrowsky, R., Feldman, E.L., Fernyhough, P., Jakobsen, J., Malik, R.A., Mizisin, A.P., Oates, P.J., Obrosova, I.G., Pop-Busui, R., Russell, J.W., Sima, A.A., Stevens, M.J., Schmidt, R.E., Tesfaye, S., Veves, A., Vinik, A.I., Wright, D.E., Yagihashi, S., Yorek, M.A., Ziegler, D. & Zochodne, D.W. (2014) Phenotyping animal models of diabetic neuropathy: a consensus statement of the diabetic neuropathy study group of the EASD (Neurodiab). *J. Peripher. Nerv. Syst.* **19**, 77-87.

Bril, V. (2014) Neuromuscular complications of diabetes mellitus. *Continuum (Minneap Minn)* **20**, 531-544.

Callaghan, B.C., Little, A.A., Feldman, E.L. & Hughes, R.A. (2012) Enhanced glucose control for preventing and treating diabetic neuropathy. *Cochrane Database Syst. Rev*. **13**, CD007543.

Choi, S., Yamada, A., Kim, W., Kim, S.K. & Furue, H. (2017) Noradrenergic inhibition of spinal hyperexcitation elicited by cutaneous cold stimuli in rats with oxaliplatin-induced allodynia: electrophysiological and behavioral assessments. *J. Physiol. Sci.* **67**, 431-438.

Christie, K.J., Webber, C.A., Martinez, J.A., Singh, B. & Zochodne, D.W. (2010) PTEN inhibition to facilitate intrinsic regenerative outgrowth of adult peripheral axons. *J. Neurosci.* **30**, 9306-9315.

Dyck, P.J. & Giannini, C. (1996) Pathologic alterations in the diabetic neuropathies of humans: a review. *J. Neuropathol. Exp. Neurol.* **55**, 1181-1193.

Feldman, E.L., Nave, K.A., Jensen, T.S. & Bennett, D.H.L. (2017) New horizons in diabetic neuropathy: mechanisms, bioenergetics, and pain. *Neuron* **93**, 1296-1313.

Furue, H. (2012) In vivo blind patch-clamp recording technique. In Okada, Y. (ed), *Patch-clamp techniques*. Springer. Tokyo. pp.171-182.

Furue, H., Narikawa, K., Kumamoto, E. & Yoshimura, M. (1999) Responsiveness of rat substantia gelatinosa neurones to mechanical but not thermal stimuli revealed by *in vivo* patch-clamp recording. *J. Physiol.* **521.2**, 529-535.

Green, A.Q., Krishnan, S., Finucane, F.M. & Rayman, G. (2010) Altered C-fiber function as an indicator of early peripheral neuropathy in individuals with impaired glucose tolerance. *Diabetes Care* **33**, 174-176.

Islam, M.S. (2013) Animal models of diabetic neuropathy: progress since 1960s. *J. Diabetes Res.* 2013, 149452.

Islam, M.S. & Wilson, R.D. (2012) Experimentally induced rodent models of type 2 diabetes. *Methods Mol. Biol*. **933**, 161-174.

Kerner, W. & Brückel, J. (2014) Definition, classification and diagnosis of diabetes mellitus. *Exp. Clin. Endocrinol. Diabetes* **122**, 384-386.

Lauria, G. & Devigili, G. (2007) Skin biopsy as a diagnostic tool in peripheral neuropathy. *Nat. Clin. Pract. Neurol.* **3**, 546-557.

Magill, C.K., Tong, A., Kawamura, D., Hayashi, A., Hunter, D.A., Parsadanian, A., Mackinnon, S.E. & Myckatyn, T.M. (2007) Reinnervation of the tibialis anterior following sciatic nerve crush injury: a confocal microscopic study in transgenic mice. *Exp. Neurol*. **207**, 64-74.

Nakamura, T., Terajima, T., Ogata, T., Ueno, K., Hashimoto, N., Ono, K. & Yano, S. (2006) Establishment and pathophysiological characterization of type 2 diabetic mouse model produced by streptozotocin and nicotinamide. *Biol. Pharm. Bull.* **29**, 1167-1174.

O'Brien, P.D., Sakowski, S.A. & Feldman, E.L. (2014) Mouse models of diabetic neuropathy. *ILAR J.* **54**, 259-272.

Ohnishi, A., O'Brien, P.C. & Dyck P.J. (1974) Studies to improve fixation of numern nerves. Part 2. Effect of time elapsed between death and glutaraldehyde fixation on relation ship of axonal area to number of myelin lamellae. *J. Neurol. Sci*. **23**, 387-390.

Park, K.K., Liu, K., Hu, Y., Smith, P.D., Wang, C., Cai, B., Xu, B., Connolly, L., Kramvis, I., Sahin, M. & He, Z. (2008) Promoting axon regeneration in the adult CNS by modulation of the PTEN/mTOR pathway. *Science* **322**, 963-966.

Preston, G.M. (1967) Peripheral neuropathy in the alloxan-diabetic rat. *J. Physiol*. **189**, 49P-50P.

Singh, B., Singh, V., Krishnan, A., Koshy, K., Martinez, J.A., Cheng, C., Almquist, C. & Zochodne, D.W. (2014) Regeneration of diabetic axons is enhanced by selective knockdown of the *PTEN* gene. *Brain* **137**, 1051-1067.

Szkudelski, T. (2012) Streptozocin-nicotinamide-induced diabetes in the rat. Characteristics of the experimental model. *Exp. Biol. Med*. **237**, 481-490.

Tesfaye, S., Boulton, A.J., Dyck, P.J., Freeman, R., Horowitz, M., Kempler, P., Lauria, G., Malik, R.A., Spallone, V., Vinik, A., Bernardi, L. & Valensi, P. (2010) Diabetic neuropathies: update on definitions, diagnostic criteria, estimation of severity, and treatments. *Diabetes Care* **33**, 2285-2293.

Tu, N.H., Katano, T., Matsumura, S., Pham, V.M., Muratani, T., Minami, T. & Ito, S. (2016) Role of c-Jun N-terminal kinase in late nerve regeneration monitored by *in vivo* imaging of thy1-yellow fluorescent protein transgenic mice. *Eur. J. Neurosci*. **43**, 548-560.

Unezaki, S., Yoshii, S., Mabuchi, T., Saito, A. & Ito, S. (2009) Effects of neurotrophic factors on nerve regeneration monitored by *in vivo* imaging in thy1-YFP transgenic mice. *J. Neurosci. Methods* **178**, 308-315.

Uta, D., Furue, H., Pickering, A.E., Rashid, M.H., Mizuguchi-Takase, H., Katafuchi, T., Imoto, K. & Yoshimura, M. (2010) TRPA1-expressing primary afferents synapse with a morphologically identified subclass of substantia gelatinosa neurons in the adult rat spinal cord. *Eur. J. Neurosci.* **31**, 1960-1973.

Van Belle, T.L., Taylor, P. & von Herrath, M.G. (2009) Mouse models for type 1 diabetes. *Drug Discov. Today Dis. Models* **6**, 41-45.

Witzemann, V. (2006) Development of the neuromuscular junction. *Cell Tissue Res*. **326**, 263-271.

Yasuda, H., Terada, M., Maeda, K., Kogawa, S., Sanada, M., Haneda, M., Kashiwagi, A. & Kikkawa, R. (2003) Diabetic neuropathy and nerve regeneration. *Prog. Neurobiol.* **69**, 229-285.

Yoshimura, M. & Jessell, T.M. (1989) Primary afferent-evoked synaptic responses and slow potential generation in rat substantia gelatinosa neurons in vitro. *J. Neurophysiol*. **62**, 96-108.

Figure legends

Figure 1. Successful establishment of type 2 diabetic mouse models. Type-2 diabetic model mice were prepared by injecting 8-week-old mice with 100 mg/kg STZ and 240 mg/kg NA twice at an interval of 2 days. Age-matched control mice were injected with vehicle. (**A**) Time course of blood glucose level before and after STZ and NA injection. Type-2 diabetic model mice and age-matched control mice at 17 weeks after STZ- and NA-injection were designated as Type 2-Db 25W and Non-Db 25W mice, respectively. Non-Db 25W (n = 5), Type 2-Db 25W (n = 7). ***p* < 0.01. In the following experiments, 10-week-old mice without treatment designated as Non-Db 10W were used as young control mice. (**B -F**) Characterization of Type 2-Db mice. (**B**) Representative images of HE staining and immunostaining with anti-insulin antibody. Scale bars: 50 μm (upper), 30 μm (lower). (**C**) Percentage of insulin-positive cells in pancreatic islets. Non-Db 10W (n = 4), Non-Db 25W (n = 3), and Type 2-Db 25W (n = 3). ***p* < 0.01. (**D**) Plasma insulin measurement in non-fasted mice. Non-Db 10W (n = 5), Non-Db 25W (n = 5), and Type 2-Db 25W (n = 5). **p* < 0.05. (**E, F**) Blood glucose (**E**) and plasma insulin (**F**) of fasted mice in a glucose tolerance test (GTT). Non-Db 10W (n = 3), Non-Db 25W (n = 4), and Type 2-Db 25W (n = 4). **p* < 0.05 and ***p* < 0.01 *vs.* Non-Db 25W. Two-tailed unpaired t-test was used in (**A**) and Non-repeated measures ANOVA followed by Dunnett's *post hoc* test was used in (**C**) - (**F**).

Addition Authors

Comment Editors

Figure 2. Behavioral and physiological characterization of Type 2-Db mice. (**A**) Withdrawal thresholds to mechanical stimuli. The data show the mean ± SEM. Non-Db 10W (n = 4), Non-Db 25W (n = 5), and Type 2-Db 25W (n = 6). ***p* < 0.01 *vs.* Non-Db 25W by non-repeated measures ANOVA followed by Dunnett's *post hoc* test. (**B**) *In vivo* extracellular recordings in the spinal dorsal horn neurons in response to cutaneous electrical stimulation applied to the ipsilateral hind limb. Examples of typical evoked-action potentials with short (upper traces) and long (lower traces) latencies from the stimulus artifact by four repetitive (1 Hz) stimulations. Arrowheads indicate discriminated evoked action potentials superimposed in the insets. The stimulus thresholds for the short and long latency-evoked responses were 0.28 and 1.5 mA, respectively.

Figure 3. Decreased innervation of the skin of type-2 diabetic mice. (**A**) Representative images of IENF in the plantar skin of untreated and axotomized mice. Immunostaining with anti-PGP9.5 antibody and counterstaining with DAPI. Scale bar: 50 μm. The enlarged figure presents the

epidermis layer (between yellow dashed lines), the counted IENF (arrow) and uncounted IENF (arrow head). Scale bar: 25 μm. (**B, C**) Quantification of the number of IENF per mm (**B**) and length of IENF (μm/100 μm^2) (**C**) in the epidermis. ***p* < 0.05, ****p* < 0.01 (n = 3/group). Non-repeated Measures ANOVA followed by Dunnett's *post hoc* test was used.

Comment Editors

Figure 4. Morphometric analysis of sciatic nerve trunk by electron microscopy. (**A**) Representative electron-micrographs of sciatic nerve of Non-Db 10W, Non-Db 25W, and Type 2-Db 25W mice without axotomy. Scale bar: 10 μm. An arrow and an arrowhead in enlarged square indicate myelinated and unmyelinated fibers, respectively. Scale bar: 5 μm. (**B-D**) Quantification of number (/mm^2) of myelinated and unmyelinated fibers (**B**), areas of axon and myelin of myelinated fibers (**C**) and the g-ratio of myelinated fibers (**D**). No significant difference among groups, n = 3/group. Non-repeated Measures ANOVA followed by Dunett's *post hoc* test was used for all statistical analyses.

Figure 5. No change in innervation to muscle by axotomy. (**A**) Representative images of NMJ structures in gastrocnemius muscle (GCM) of *thy1*-YFP mice before and 11 weeks after axotomy. An arrow and an arrowhead indicate endplates with and without innervation, respectively. Scale bar: 100 μm. (**B**) Percentage of normal NMJ counted in GCM. Endplates were visualized by α-BTX and counted as described in "Materials and methods."

Figure 6. Delay of nerve reinnervation and functional recovery after sciatic nerve axotomy. (**A**) Representative images of reinnervation of proper plantar digital nerves before and 5, 7, and 11 weeks after axotomy. Arrowheads indicate intact and regenerating nerves. (**B**) Number of reinnervated proper plantar digital nerves. Non-Db 10W (n = 4), Non-Db 25W (n = 5), and Type 2-Db 25W (n = 6). ***p* < 0.05 and ****p* < 0.01 *vs*. Non-Db 25W. (**C**) Time courses of withdrawal thresholds to mechanical stimuli after axotomy. Withdrawal thresholds were recorded by use of von Frey filament stimulation, as described in "Materials and methods." A mechanical force of 4 g was used as the cut-off value. The values after axotomy are indicated as the mean ± SEM. Non-Db 10W (n = 4), Non-Db 25W (n = 5), and Type 2-Db 25W (n = 6); ***p* < 0.05 and ****p* < 0.01 *vs*. Non-Db 25W. Non-repeated measures ANOVA followed by Dunnett's *post hoc* test was used for all statistical analyses.

Figure 7. Enhancement of functional recovery by PTEN inhibition after axotomy. (**A, B**) Western blot of PTEN protein in L4 - L6 DRGs individually prepared from naive and Type 2-Db mice. Vinculin was used as the loading control. The expression level of PTEN was normalized by vinculin. $^{**}p < 0.01$ by unpaired t-test (n = 3). (**C**) Effect of PTEN inhibitor on functional recovery after axotomy. PTEN inhibitor (200 nM) was continuously administered into a silicon tube of Non-Db and Type 2-Db mice with an osmotic pump for 4 weeks immediately after axotomy. Mechanical sensitivity was recorded by use of von Frey filaments, as described in the legend for Fig. 3C. The data show the mean ± SEM, n = 6/group. $^{\#\#}p < 0.01$, Type 2-Db-PTEN inh. *vs*. Type 2-Db veh; $^{*}p < 0.05$, Non-Db-PTEN inh. *vs.* Non-Db-veh, by two-way non-repeated Measures ANOVA followed by Tukey's *post hoc* test. (**D**) Representative images of whole mount L5 DRGs after Fluoro-ruby introduction. Scale bar: 200 µm. (**E**) Number of Fluoro-ruby-labelled sensory neurons counted in L4-6 DRGs. n= 3 mice/group; $^{**}p \leq 0.01$; $^{\#}p \leq 0.05$ and $^{\#\#}p \leq 0.01$. Two-way non-repeated Measures ANOVA followed by Tukey's post hoc test.

Comment Editors

Addition Authors

Comment Editors

Fig1

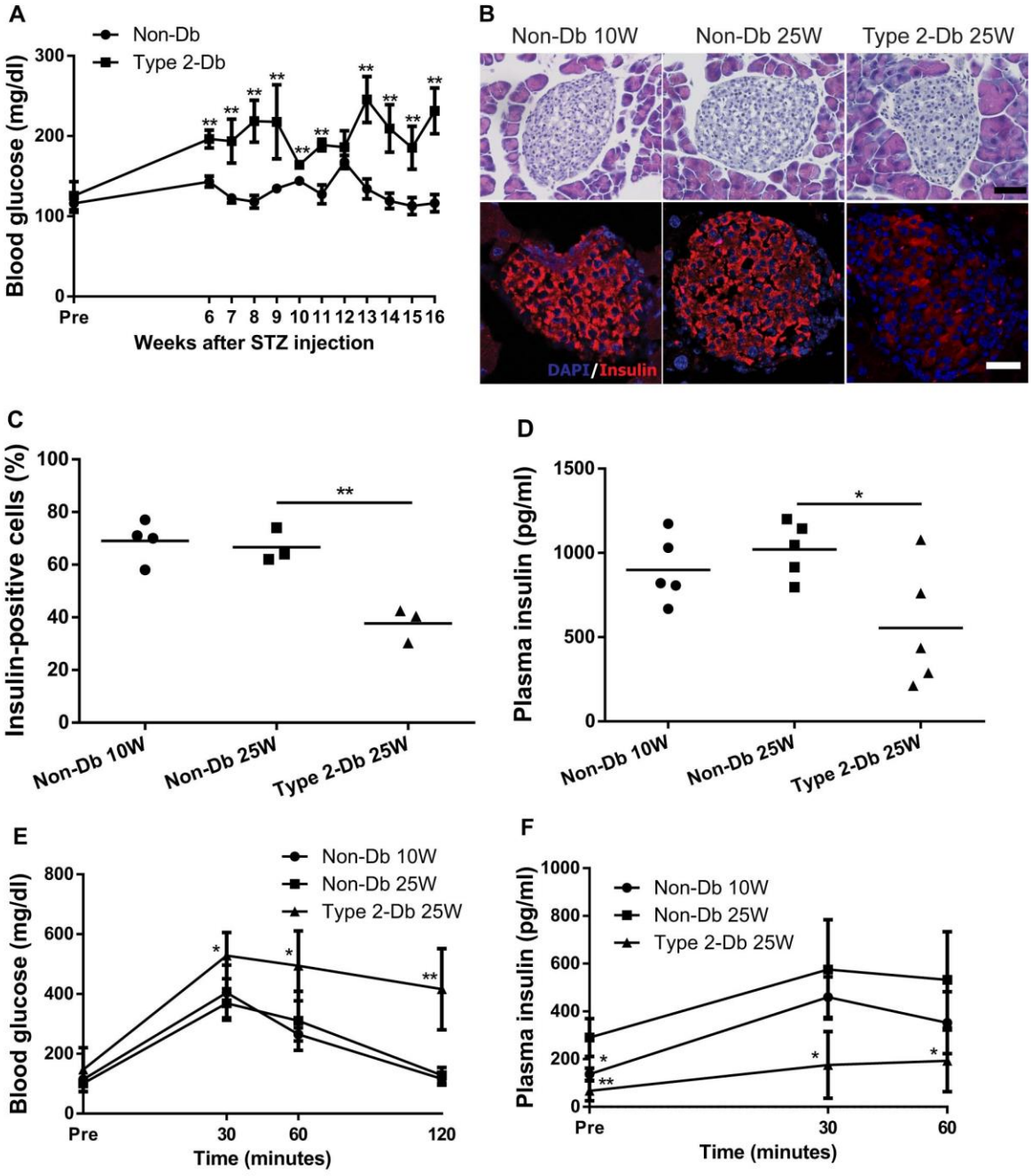
A
Non-Db
Type 2-Db
Blood glucose (mg/dl)
Pre
6 7 8 9 10 11 12 13 14 15 16
Weeks after STZ injection
B
Non-Db 10W
Non-Db 25W
Type 2-Db 25W
DAPI/Insulin
C
Insulin-positive cells (%)
Non-Db 10W
Non-Db 25W
Type 2-Db 25W
D
Plasma insulin (pg/ml)
Non-Db 10W
Non-Db 25W
Type 2-Db 25W
E
Non-Db 10W
Non-Db 25W
Type 2-Db 25W
Blood glucose (mg/dl)
Pre
30
60
120
Time (minutes)
F
Non-Db 10W
Non-Db 25W
Type 2-Db 25W
Plasma insulin (pg/ml)
Pre
30
60
Time (minutes)

Fig2

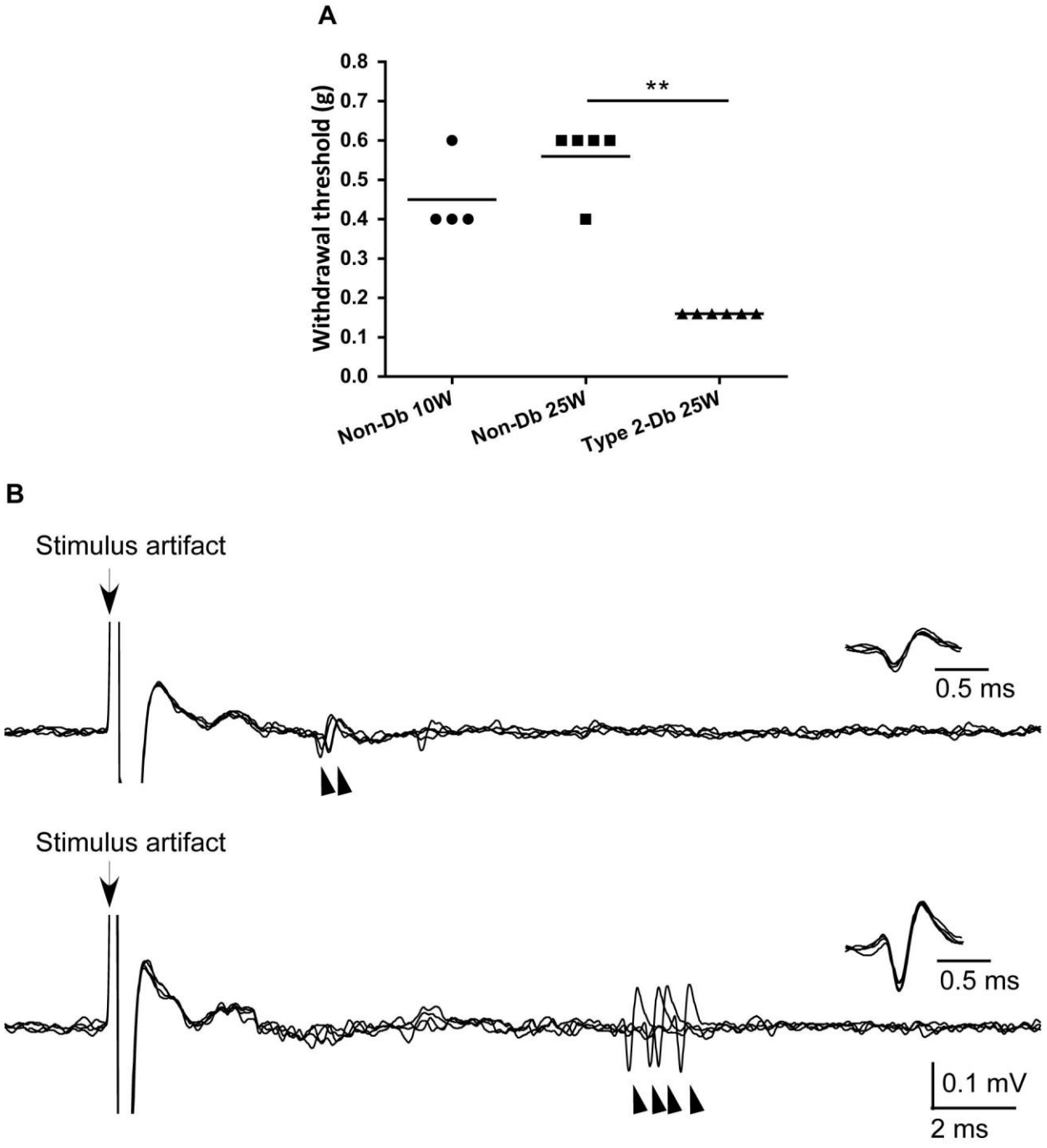
A
Withdrawal threshold (g)
0.8
0.7
0.6
0.5
0.4
0.3
0.2
0.1
0.0
**
Non-Db 10W
Non-Db 25W
Type 2-Db 25W
B
Stimulus artifact
0.5 ms
Stimulus artifact
0.5 ms
0.1 mV
2 ms

Fig3

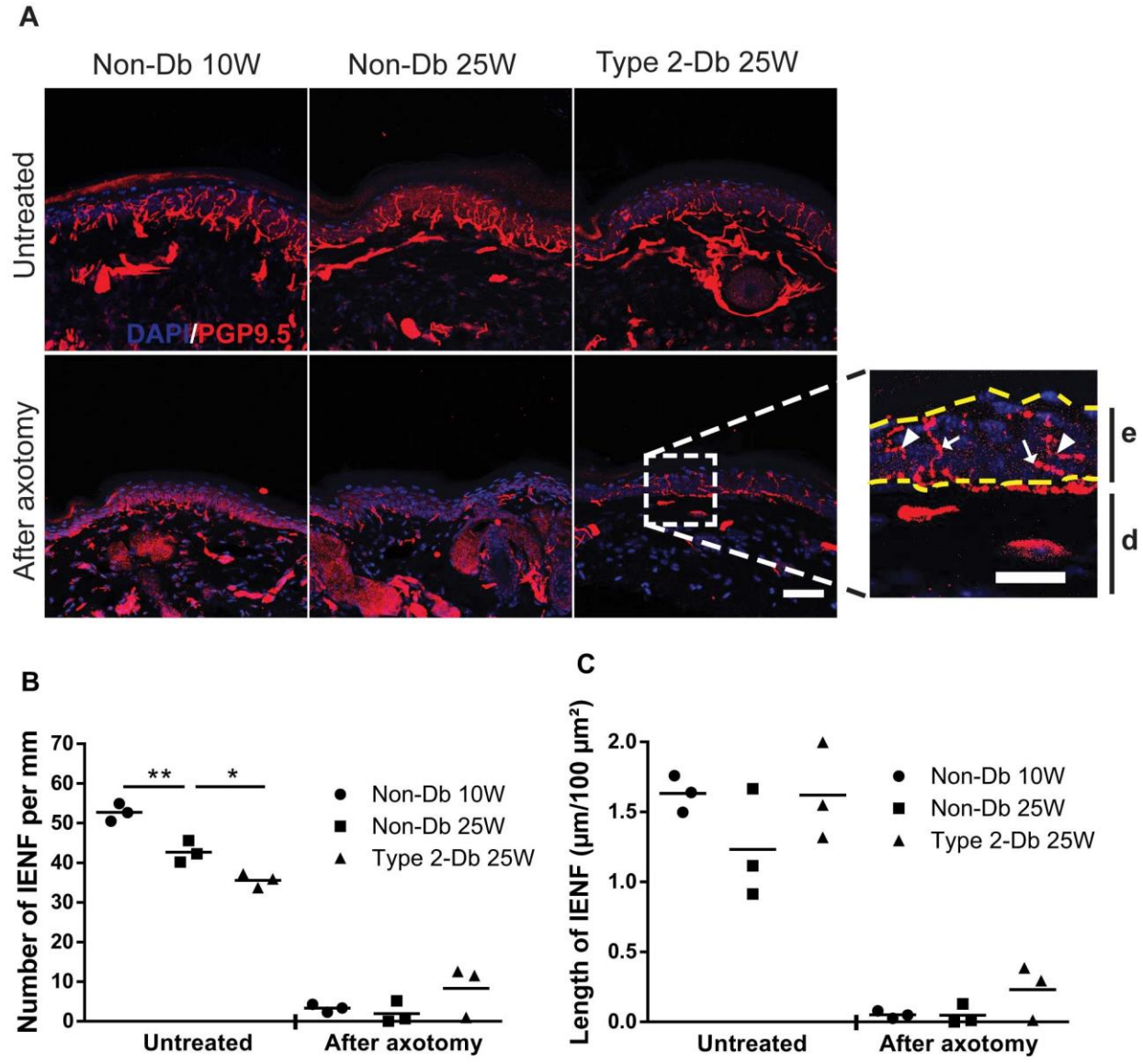
A
Non-Db 10W
Non-Db 25W
Type 2-Db 25W
Untreated
After axotomy
DAPI/PGP9.5
e
d
B
Number of IENF per mm
70
60
50
40
30
20
10
0
**
*
Non-Db 10W
Non-Db 25W
Type 2-Db 25W
Untreated
After axotomy
C
Length of IENF (μm/100 μm²)
2.0
1.5
1.0
0.5
0.0
Non-Db 10W
Non-Db 25W
Type 2-Db 25W
Untreated
After axotomy

Fig4

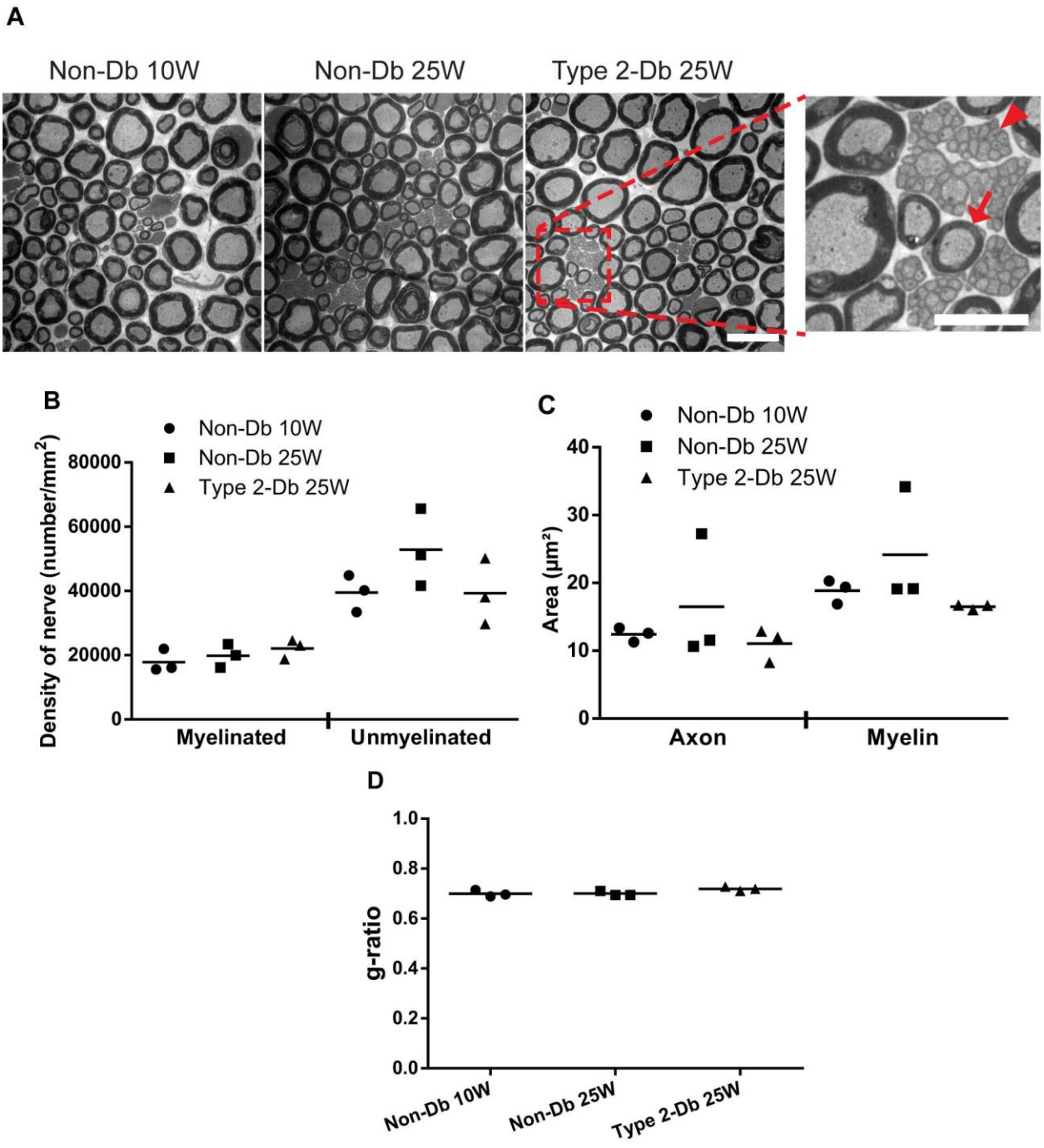
A
Non-Db 10W
Non-Db 25W
Type 2-Db 25W
B
Density of nerve (number/mm²)
80000
60000
40000
20000
0
Non-Db 10W
Non-Db 25W
Type 2-Db 25W
Myelinated
Unmyelinated
C
Area (μm²)
40
30
20
10
0
Non-Db 10W
Non-Db 25W
Type 2-Db 25W
Axon
Myelin
D
g-ratio
1.0
0.8
0.6
0.4
0.2
0.0
Non-Db 10W
Non-Db 25W
Type 2-Db 25W

Fig5

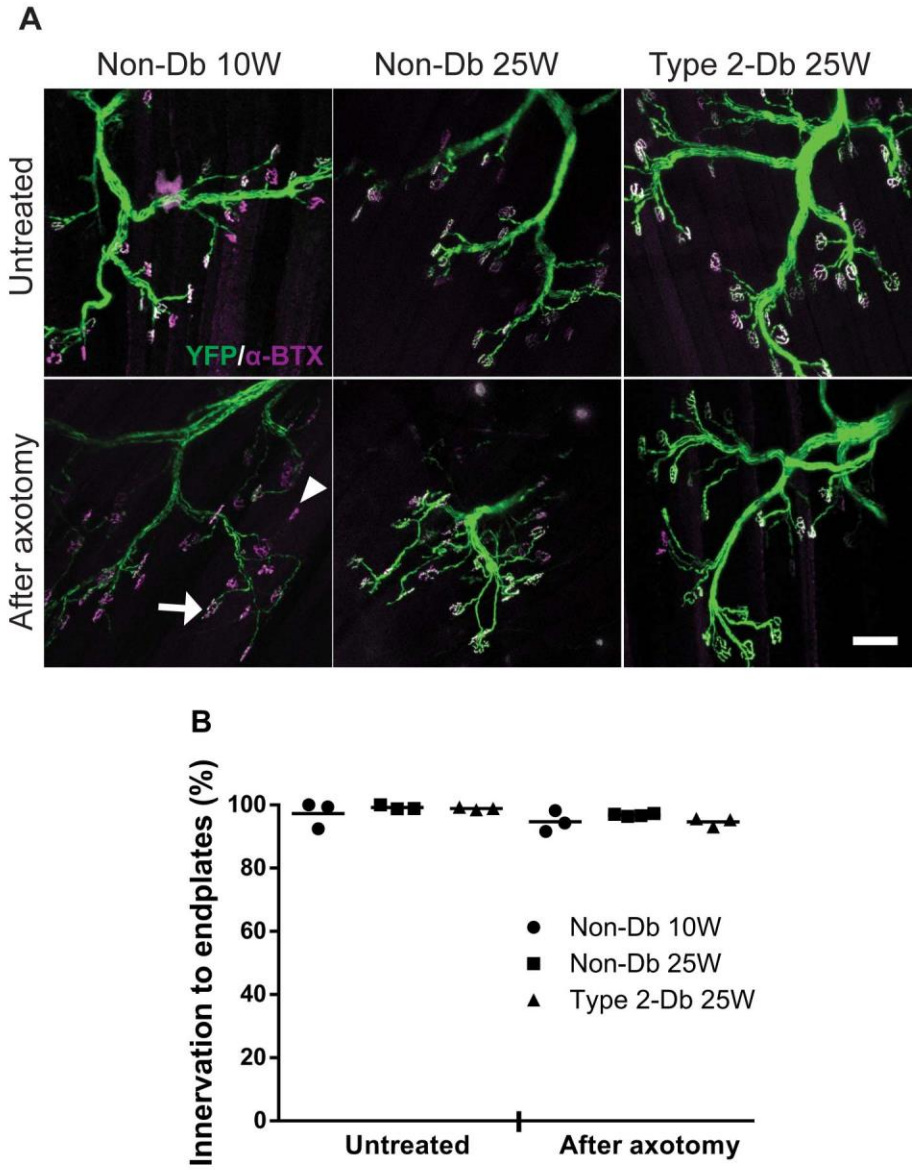
A
Non-Db 10W
Non-Db 25W
Type 2-Db 25W
Untreated
After axotomy
YFP/α-BTX
B
Innervation to endplates (%)
100
80
60
40
20
0
Non-Db 10W
Non-Db 25W
Type 2-Db 25W
Untreated
After axotomy

Fig6

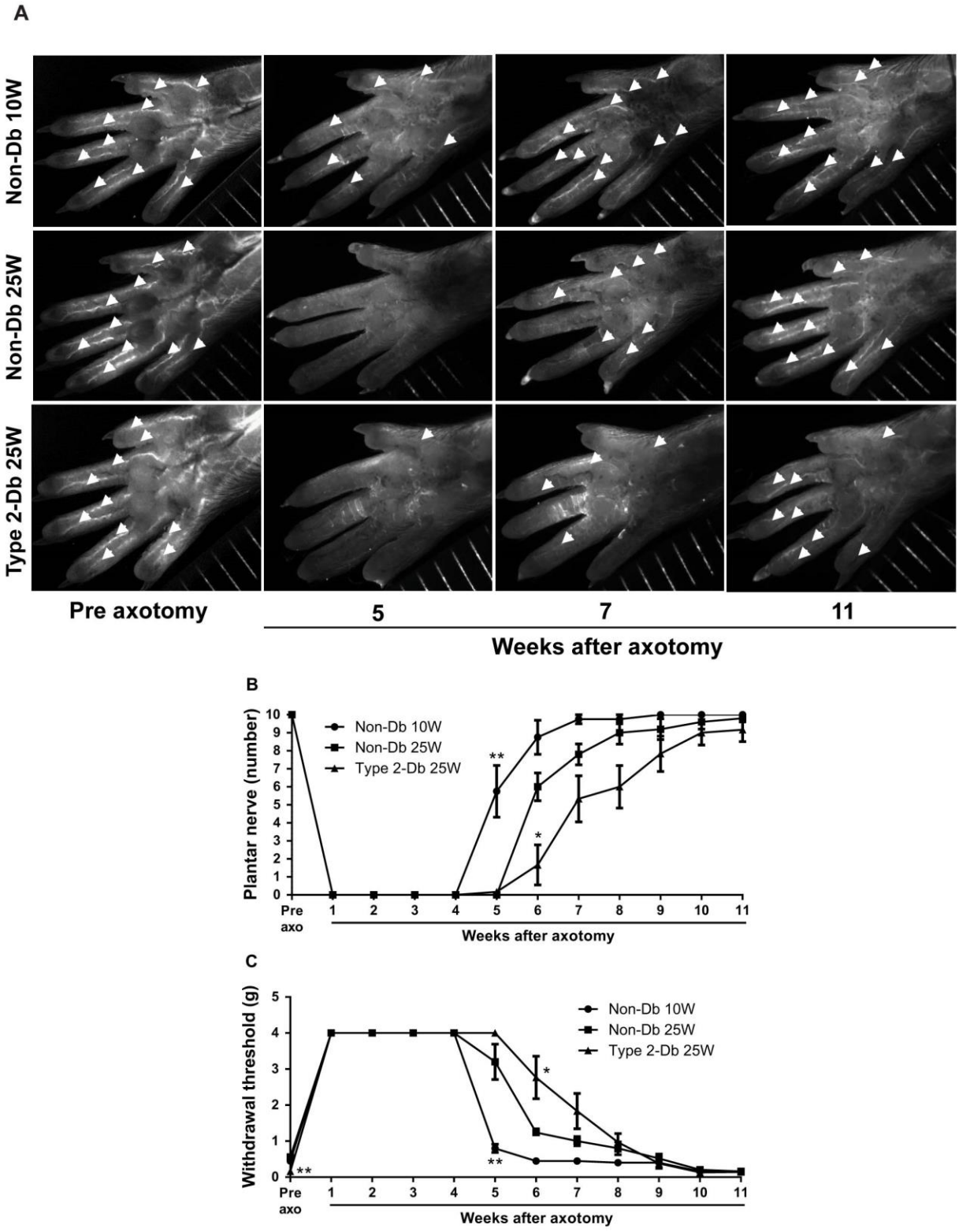
A
Non-Db 10W
Non-Db 25W
Type 2-Db 25W
Pre axotomy
5
7
11
Weeks after axotomy
B
Plantar nerve (number)
Non-Db 10W
Non-Db 25W
Type 2-Db 25W
Pre axo
Weeks after axotomy
C
Withdrawal threshold (g)
Non-Db 10W
Non-Db 25W
Type 2-Db 25W
Pre axo
Weeks after axotomy

Fig7

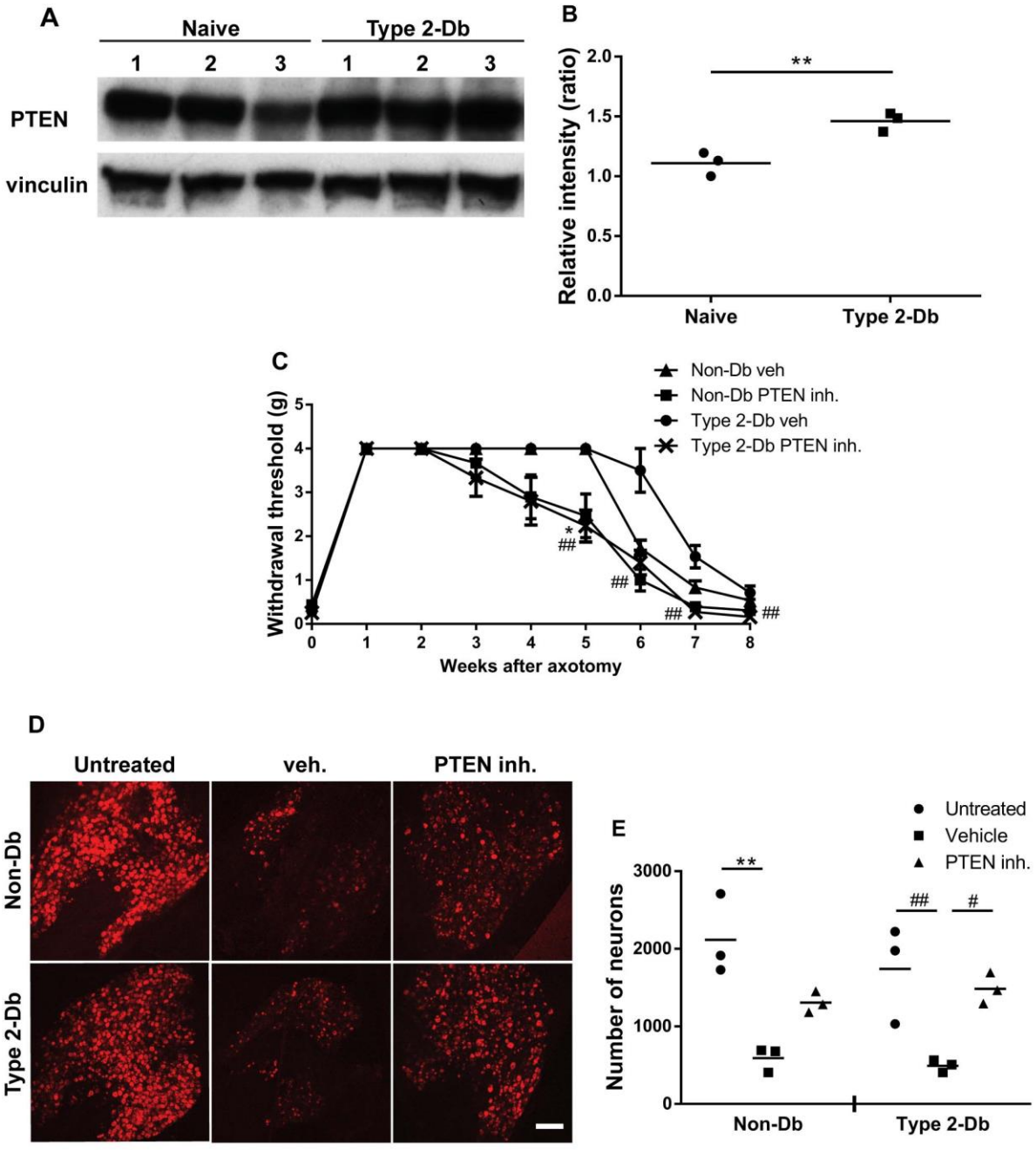
A
Naive
Type 2-Db
1 2 3 1 2 3
PTEN
vinculin
B
Relative intensity (ratio)
2.0
1.5
1.0
0.5
0.0
**
Naive
Type 2-Db
C
Non-Db veh
Non-Db PTEN inh.
Type 2-Db veh
Type 2-Db PTEN inh.
Withdrawal threshold (g)
Weeks after axotomy
D
Untreated
veh.
PTEN inh.
Non-Db
Type 2-Db
E
Untreated
Vehicle
PTEN inh.
Number of neurons
3000
2000
1000
0
**
##
#
Non-Db
Type 2-Db